The Influence of Oxygen Additions on Argon-Shielded Gas Metal Arc Welding Processes

Mass flow, electric potential and temperature in the arc column were found to be little affected by additions of 5% or less oxygen

BY P.G. JÖNSSON, A.B. MURPHY AND J. SZEKELY

ABSTRACT. It has been observed experimentally that small additions of oxygen to the argon shielding gas affect the general operation of GMAW processes. By theoretically modeling the arc column, it is shown that the addition of 2 to 5% oxygen to argon has an insignificant effect on the arc characteristics. This corresponds to the minor changes in the thermophysical transport and thermodynamic properties caused by the oxygen addition. Therefore, it is concluded that the addition of oxygen to the argon shielding gas mainly affects the anode and the cathode regions. From the literature, it was found that the formation of oxides initiates arcing at the cathode and decreases the movement of the cathode spots. These oxides can also improve the wetting conditions at the workpiece and the electrode. Finally, oxygen is found to affect the surface tension gradient and thereby the convective flow of liquid metal in the weld pool.

Introduction

In the early fifties, it was found that the addition of small amounts of oxygen to the argon shielding gas in gas metal arc welding (GMAW) allowed the range of weldable materials to be extended from aluminum and stainless steel to include carbon steels (Ref. 1). Today, oxygen additions to the shielding gas are widely used in many applications of the GMAW process. It is commonly believed that oxygen reduces the surface tension of the metal and improves the arc stability and arc root behavior. So far, no information has been published in the open literature regarding the effects of oxygen additions on the characteristics of the arc column. The main reasons for this have been the difficulty in obtaining high-temperature data for thermophysical properties for an argon-oxygen mixture, and the lack of a gas metal arc model. However, recent developments at CSIRO have increased the reliability of calculations of the thermophysical properties for a large number of gas mixtures. Also, some recent work in our laboratory at MIT has led to the development of the first model representing the gas metal arc.

The main purpose of this article is to present the results of our study of the effects of oxygen addition on the characteristics of an argon arc for GMAW of iron and aluminum. We shall also relate these findings to previous studies of the importance of oxygen in the anode and cathode region, in order to give a more complete description of the influence of oxygen additions on the performance of the GMAW process.

One section of the article describes the GMAW process, and another section summarizes previous work on the influence of oxygen addition on arc welding processes. We then describe the method of calculation of the thermophysical properties and the calculation of the arc characteristics. Finally, by examining our calculated results in conjunction with previously reported work, we discuss the influence of oxygen additions on argon-shielded GMAW processes.

KEY WORDS

Oxygen Additions
Argon Shielding Gas
GMAW
Arc Characteristics
Gas Properties
Arc Column
Theoretical Model
Computational Model
Oxide Formation
Surface Tension

Background

Figure 1 shows the main components of the GMAW system, which is seen to consist of the consumable electrode (anode), the anode-fall region, the arc column, the cathode-fall region and the workpiece (cathode). The figure also includes the gas-shielding nozzle, through which the shielding gas is supplied to the arc.

When an arc is struck between the

P. G. JÖNSSON is with MEFOS, Luleå, Sweden. A. B. MURPHY is with CSIRO, Division of Applied Physics, Lindfield, Australia. J. SZEKELY is with Department of Materials Science and Engineering, Massachusetts Institute of Technology, Cambridge, Mass.

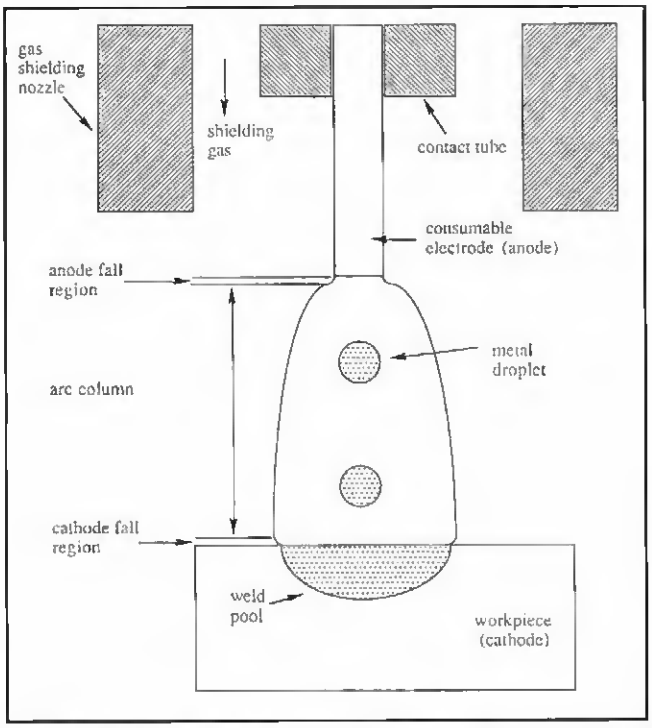

Fig. 1 — The gas metal arc welding system.

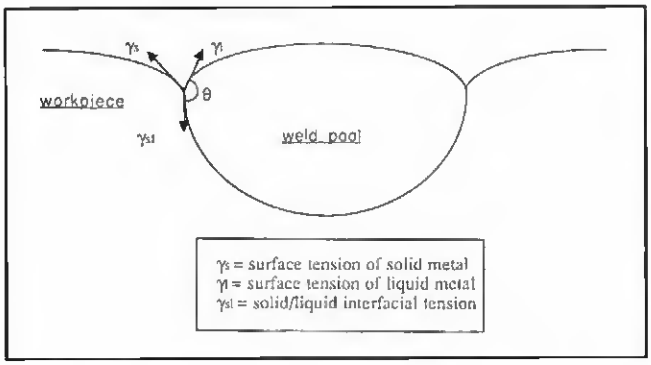

Fig. 2 — Definition of the wetting contact angle, q.

anode and the cathode, a current flows through the electric discharge between the electrodes. The arc current is spread laterally and a jet is formed which gives rise to a flow in the direction of the cathode (workpiece). The gas impinges on the workpiece and is spread in a direction parallel to the workpiece. Also, the current distribution at the anode gives rise to a high heat generation in the near anode area, which results in a rapid melting of the consumable electrode. Droplets are formed at the melted tip, detach from the electrode, and are transferred to the workpiece under the influence of arc forces. The melted droplets solidify at the workpiece and form the welded joint.

Of the two workpiece materials discussed in this article, aluminum is known to be a nonthermionic cathode characterized by a mobile cathode spot (Ref. 2). It is not clear, on the other hand, whether thermionic or nonthermionic emission of electrons occurs from iron cathodes (Ref. 3). However, the following observations indicate that iron shows more of a nonthermionic than a thermionic cathode behavior. First, Essers and Walter (Ref. 4) found that the calculated value of the current density, as a result of thermionic emission, is very low. Second, the mobile cathode spot behavior usually observed for nonthermionic cathodes is also observed in GMAW of steel (Ref. 3). Third, calculated values of the current density, as a result of thermionic emission, have shown good agreement with experimental data on materials with boiling points of at least 4000 K (Ref. 3) (the boiling point of iron is 3343 K (Ref. 5)). Based on these findings, iron will be treated as a nonthermionic electron emitter in this study.

Previous Work

Initially, some general observations of the influence of oxygen on the GMAW process will be presented. Thereafter, the review of the importance of oxygen in GMAW operations will be separated into two main parts: 1) the effects due to oxide formation; and 2) the effects due to the influence on surface tension gradients of liquid metals. In doing this, we choose to include results from other arc welding processes for the sake of completeness.

In general, experimental observations have shown that oxygen additions to a shielding gas have a major impact on the weld pool, leading to an increased length, width, volume and section (Ref. 6). However, use of an oxidizing gas can cause some ferrous metals to become porous, and therefore reducing elements are usually added to the electrode to compensate for this effect (Ref. 7). Also, it has been found that addition of too high a proportion of oxygen, 7 to 8% or more, to the argon shielding gas increases slag formation and leads to firmer attachment of the slag to the surface (Ref. 8).

It has also been found that an improvement in the toughness of ferritic steels may be obtained by increasing the oxidizing potential through addition of up to 2% oxygen to the argon shielding gas (Ref. 9). Moreover, Francis, *et al.* (Ref. 10), found that the use of an argon-based gas with 2 to 4% oxygen and the composition of the welding wire, are critical in achieving a high fracture toughness. According to the authors, the fracture toughness is determined by the amount of acicular ferrite formed, which is dependent on the number and size of oxide inclusions.

Effects Due to Oxide Formation

It is commonly believed that nonthermionic cathodes operate by the continuous formation and decay of several small electron-emitting sites (cathode spots, Refs. 3, 11). The site lifetime for thick oxide films on mild steel has been shown to be as low as 1 ns (Ref. 12). The oxides, formed by reactions between oxygen and workpiece elements, are believed to act as a source of electrons, because they usually have a lower work function than the metal (Ref. 13). The oxides are also thought to be charged by incident positive ions and to emit electrons by a tunneling mechanism and a switching mechanism for oxide thicknesses smaller than 5 nm and larger than 10 nm, respectively (Ref. 14). For welding arcs acting on an oxidized steel workpiece, each emitting site has been found to carry up to 1 A of current (Ref. 15). The emitting sites are also said to move outward toward fresh oxide and to consume it at a certain rate (Ref. 16). The area over which the oxide is removed increases with an increase in the change in the cathode voltage drop (Ref. 17).

The mobility of nonthermionic cathode spots is undesirable in GMAW, be-

cause it causes arc instabilities, which makes welding more difficult (Ref. 15). For the case of an aluminum workpiece material, it has been shown that the presence of a relatively thick oxide layer tends to restrict the mobility of the cathode spot (Ref. 2). According to Lancaster (Ref. 2), the thickness of the metal oxide increases if oxygen is added to an argon shielding gas. He used this reasoning to explain the observation of a lower mobility of the electron emitting sites for GMAW of steel when small amounts of oxygen were added to the argon shielding gas.

Oxides, in the form of nonmetallic inclusions formed by reactions between oxygen and alloying elements, have also been shown to affect the cathode behavior. Hancox (Ref. 18) found that the arcing was initiated by the dielectric charging and breakdown of insulating alumina inclusions at the cathode surface. A similar reason for arc ignition was reported by Pfeil and Griffiths (Ref. 19), who showed that the ignition took place at cathode inclusions of high resistivity.

Further evidence that the influence of oxygen is important is given by Doan and Myer (Ref. 20), who showed that an arc could not be struck between two very pure iron electrodes if oxygen was removed from the argon gas. The use of very pure argon gas has also been shown to result in unstable metal transfer during GMAW of aluminum (Ref. 21).

Oxygen additions are also known to promote the wetting of the workpiece by the weld pool (wetting-in of the weld pool) (Ref. 22). In general, good wetting conditions are achieved if the contact angle θ, defined in Fig. 2, is low. Bradstreet (Ref. 23) found that when oxygen was present in the shielding gas, the value of this contact angle decreased due to the presence of a film of SiO_2 on the molten steel. It was believed that silica acted as wetting agent, due to the low value of its surface tension (0.2 to 0.26 Nm^{-1}, Ref. 23) compared to that of steel (1.7 to 1.9 Nm^{-1}, Refs. 24, 25), and thereby improved the wetting conditions.

Effects Due to Influence on Surface Tension of Liquid Metal

Surface tension gradients $d\gamma/dT$, where γ is the surface tension of the liquid metal and T is the temperature, are known to give rise to thermocapillary (Marangoni) convection, cause high surface velocities, and play a major role in determining the heat transfer to the liquid-solid interface in weld pools (Ref. 26). In early theoretical investigations of weld pools, in which the value of $d\gamma/dT$ was assumed to be constant, it was found that the surface-tension-driven flow had a profound effect on the weld pool shape both in GMAW (Refs. 27–29) and in gas tungsten arc welding (GTAW) systems (Refs. 30–36). The assumption that the value of the surface tension gradient was constant, which was made due to the lack of experimental or theoretical data for $d\gamma/dT$, was a serious limitation, since Heiple and Roper (Ref. 37) proposed that surface-active elements could actually change the sign of the surface tension gradient, and thereby the direction of the flow.

The first semi-empirical theoretical relationship between the surface tension gradient and the temperature and activity of the surface-active element was derived from Gibbs and Langmuir isotherms by Sahoo, *et al.* (Ref. 38). If oxygen is taken as the surface-active element, the surface tension gradient can be expressed as

$$\frac{d\gamma}{dT} = -A - R\Gamma_0 \ln\left(1+K_{seg}\right) - \frac{K_{seg}\, a_0}{\left(1+K_{seg}\, a_0\right)} \frac{\Gamma_0 \Delta H^0}{T} \qquad (1)$$

where A is a constant in the surface tension coefficient, R is the gas constant, Γ_o is the surface excess at saturation, K_{seg} is the equilibrium constant for segregation, a_o is the activity of oxygen and ΔH^0 is the standard heat of adsorption.

The surface tension gradient is negative for most pure metals and the corresponding surface-tension-driven flow in the weld pool is directed towards the edges of the weld pool as shown in Fig. 3A. The addition of oxygen to an iron melt can change the sign of the surface tension gradient to positive (Ref. 38). This will change the corresponding flow pattern in the weld pool so that the surface velocities are directed toward the center of the weld pool, as illustrated in Fig. 3B.

Recent mathematical models of the GTAW system by Zacharia, *et al.* (Refs. 39–42), used Equation 1 to predict the influence of surface-active elements and temperature distribution on the weld pool geometry. It was quantitatively

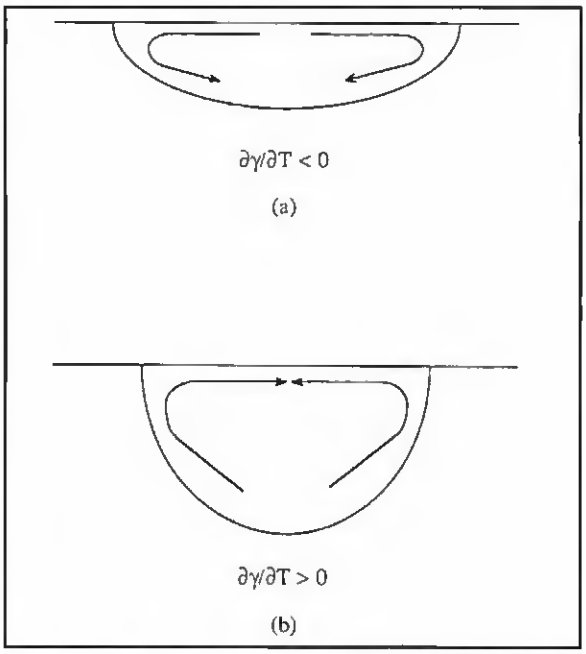

Fig. 3 — Convection due to thermocapillary forces at: A — a negative surface tension gradient (pure metal); B — a positive surface tension gradient (metal containing oxygen).

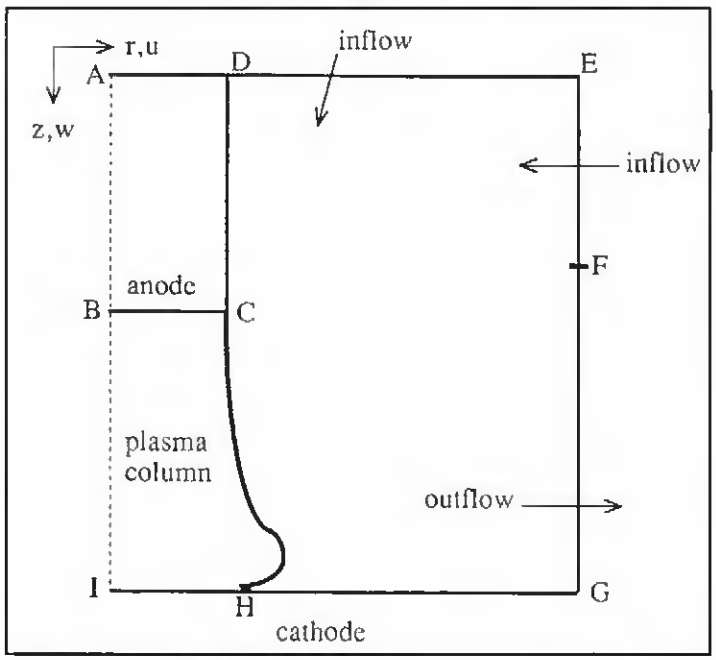

Fig. 4 — Outline of integration domain.

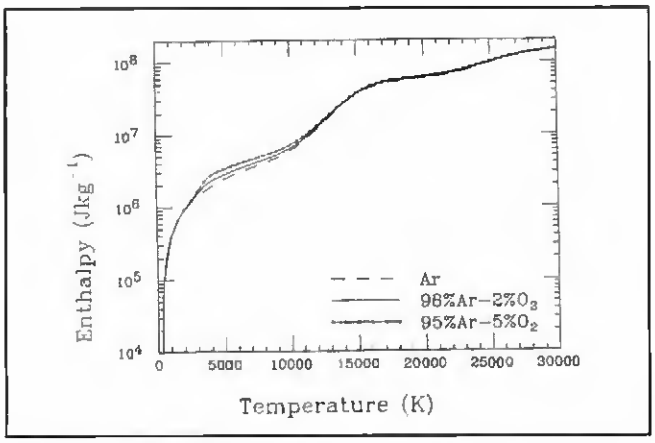

Fig. 5 — The enthalpy as a function temperature.

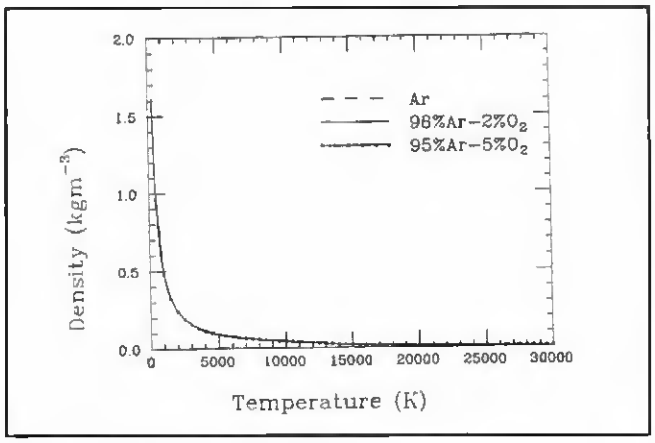

Fig. 6 — The density as a function of temperature.

demonstrated that the base metal composition is indeed critical in controlling the weld bead shape.

Theoretical Modeling

Calculation of Thermophysical Gas Properties

The model of the arc column that we use requires values of the density, enthalpy, specific heat, viscosity, thermal conductivity, electrical conductivity, and radiative emission coefficients as a function of temperature for pure argon and mixtures of argon and oxygen. The radiation loss terms for both argon and the argon-oxygen mixtures are taken from experimental data for argon of Evans and Tankin (Ref. 43). The radiation loss terms for the argon-oxygen mixtures are assumed to be the same as for argon, because the total radiation of oxygen is of the same order of magnitude as for argon (Ref. 44) and only 2 to 5% oxygen is added. The other quantities are calculated using a code designed to calculate the equilibrium compositions and thermophysical properties of nonionized gas mixtures (Refs. 45, 46), which has been modified by Kovitya (Refs. 47–49) to allow for treatment of ionized gases.

All calculations are performed assuming local thermodynamic equilibrium. The initial step in the determination of the thermophysical properties is the calculation of the equilibrium composition of the gas or gas mixture, which is done using the principle of minimization of the Gibbs free energy. The species considered are Ar, Ar^+, Ar^{++}, Ar^{+++}, O_2, O_2^+, O^-, O^+, O^{++}, O^{+++}, and the electron. The presence of metallic species is neglected, since the focus is on studying the effect of oxygen additions on the argon plasma. The required partition functions for the considered species are calculated from the data tabulated by Moore (Ref. 50) for neutral and positively charged monoatomic species, and from data given in the JANAF tables (Ref. 51) for other species. The Debye-Hückel correction is applied, as described by Kovitya (Ref. 49).

The density of the mixture at temperature T and pressure P is calculated using

$$\rho = \frac{P\sum_j x_j M_j}{RT} \qquad (2)$$

where x_j is the mole fraction and M_j is the molecular weight of the jth species. The enthalpy and specific heat of the mixture are calculated using the expressions given by Kovitya (Ref. 49), which includes terms for the Debye-Hückel correction.

The transport coefficients; viscosity, thermal conductivity, and electrical conductivity; are calculated using the Chapman-Enskog method (Refs. 52–54). Details of the calculations are given by Murphy (Ref. 55). The thermal conductivity is calculated as the sum of the contributions due to the translational, internal, and reaction components. The translational component is further broken down into contributions due to heavy particle and electron motion; the electron component is calculated to a third level of approximation, while the heavy particle component is calculated to a second level. Note that the first level of approximation for the thermal conductivity is identically zero. The electrical conductivity is calculated to a third level of approximation, neglecting the influence of ion transport. The viscosity is calculated to a first level of approxima-

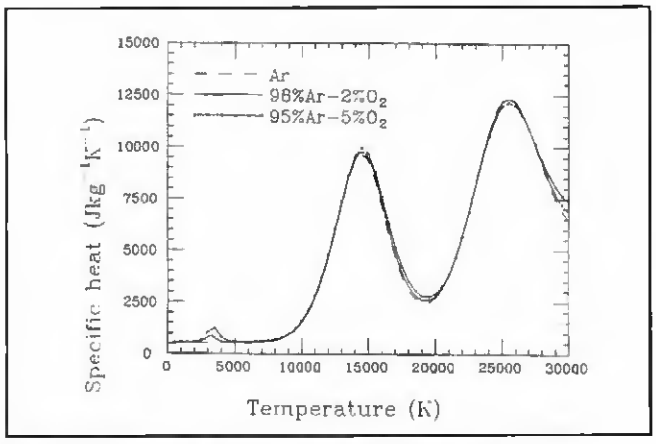

Fig. 7 — The specific heat as a function of temperature.

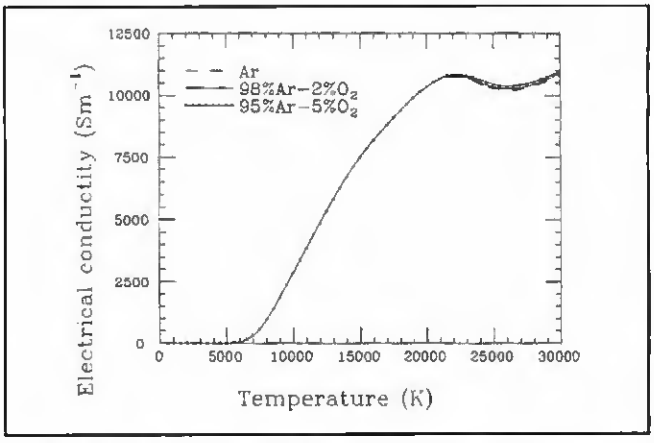

Fig. 8 — The electrical conductivity as a function of temperature.

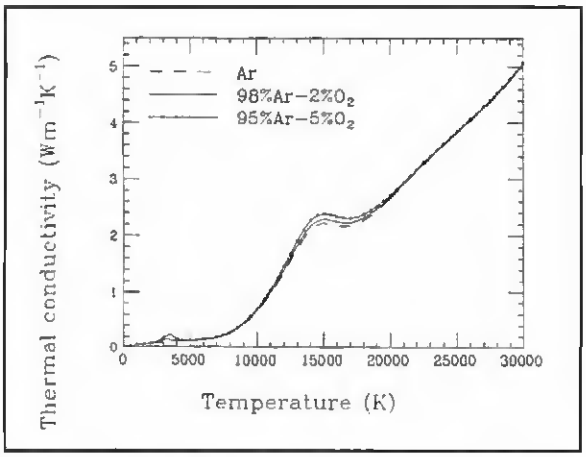

Fig. 9 — The thermal conductivity as a function of temperature.

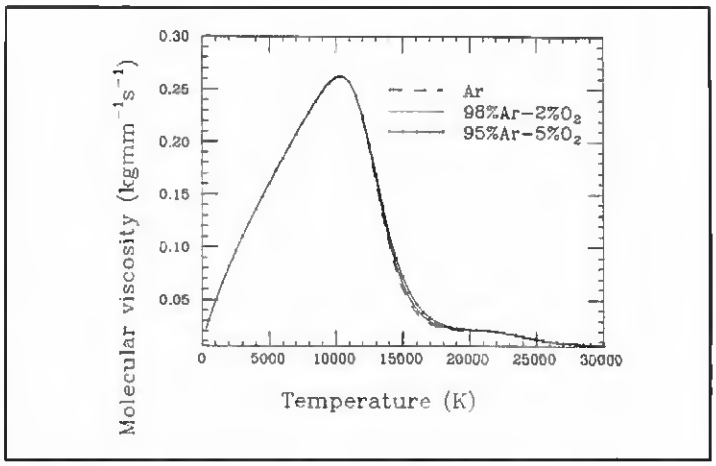

Fig. 10 — The molecular viscosity as a function of temperature.

tion. Devoto (Refs. 56, 57) has verified that the levels of approximation used give results accurate to within 1% for argon, except for the electrical conductivity at very low levels of ionization. Since the electrical conductivity is very low under these conditions, the absolute error is always small (less than 200 5m^{-1}).

The collision integrals, integrals over a Maxwellian distribution of the collision cross-sections for interactions between the various species, are required to calculate the transport coefficients. Most of the integrals are calculated from the intermolecular potentials given by Aubreton, *et al.* (Ref. 58). However, in a number of cases improved data are used. The collision integrals for the Ar-Ar and Ar-O_2 interactions are respectively calculated from the HFDTCS2 potential given by Aziz and Slaman (Ref. 59) and the E5M5V potential given by Pirani and Vecchiocattivi (Ref. 60). The charge-exchange cross-section required in the calculation of the collision integrals for the O-O interaction is taken from the experimental results of Rutherford and Vroom (Ref. 61). The collision integral tabulations of Levin, *et al.* (Ref. 62), and Stallcop, *et al.* (Ref. 63), are used directly for the O-O and O^+-O interactions respectively. Finally, the collision integrals for electron-neutral interactions are treated by numerical integration of the momentum-transfer cross-section data presented by Itikawa (Refs. 64, 65), supplemented at low and high energies by further data from Itikawa's sources.

Our values for the thermodynamic properties of argon and argon-oxygen mixtures are expected to be accurate to within a few percent. The main source of uncertainty in the calculation of transport properties is in the collision integrals. These are generally well defined in the case of interactions between argon species, leading to good agreement, within a few percent, between recent calculations by different authors of the transport properties of argon (Ref. 55). There is, in contrast, considerable variation between published collision integral data for some interactions between oxygen species, particularly the O^+-O interaction. However, the data here are expected to be considerably more reliable than less-recent values (Ref. 55). This, and the small concentrations of oxygen considered in the calculations, means that our transport properties of argon-oxygen mixtures will not be significantly less accurate than our results for pure argon.

The calculated thermophysical properties for the shielding gases considered in this paper are shown, and discussed later.

Description of Arc Model

A two-dimensional steady-state mathematical model has been developed to predict properties such as temperature, velocity, and voltage in the gas metal arc. In an earlier study, the model was applied to GMAW of aluminum in an argon atmosphere (Ref. 66). Calculated values for temperatures, at an axial location halfway between the electrode and the workpiece, were found to differ by 0 to 6.1% and 0 to 3.8% in comparison with

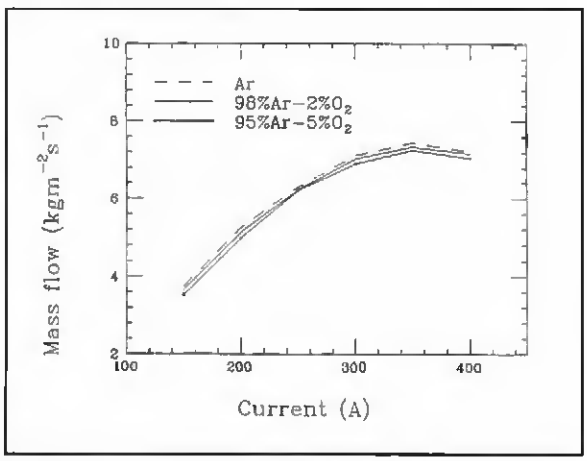

Fig. 11 — The maximum value of the mass flow plotted as a function of the current.

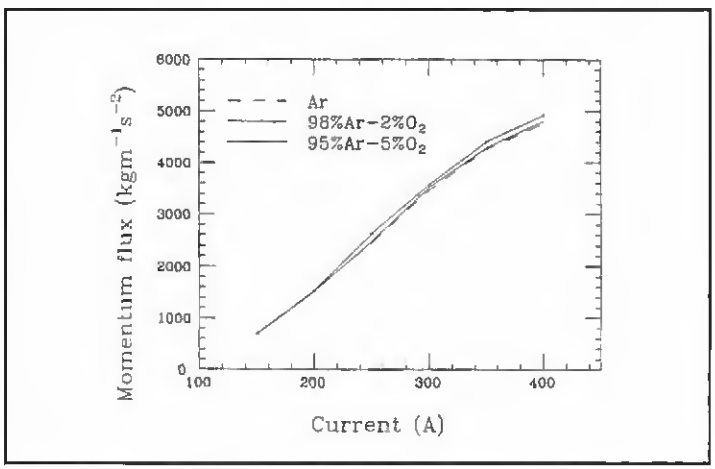

Fig. 12 — The maximum value of the momentum flux as a function of the current.

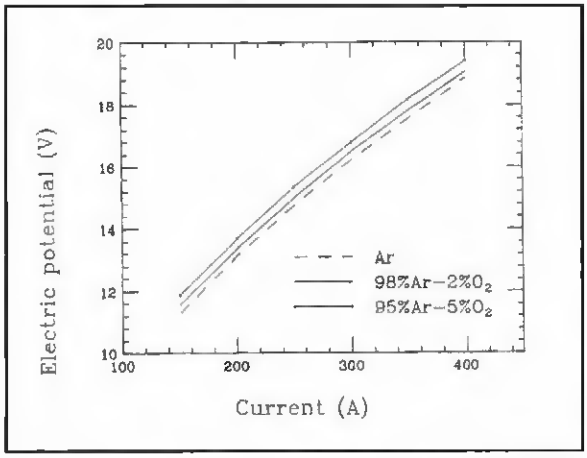

Fig. 13 — The maximum value of the electric potential as a function of the current.

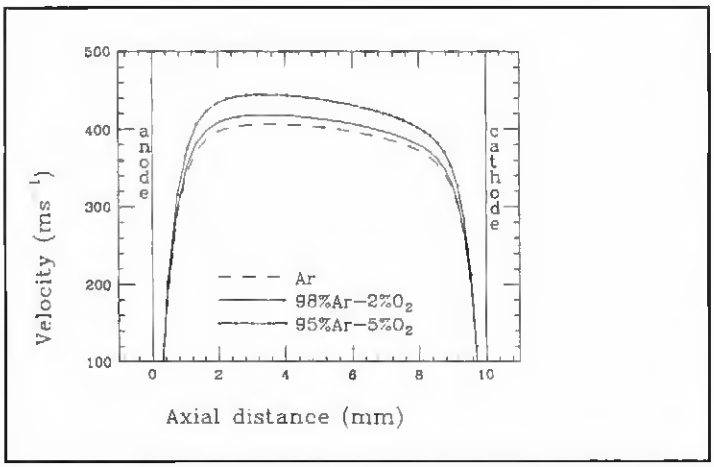

Fig. 14 — The axial velocity at the center of the arc as a function of the axial distance from the anode.

spectroscopically measured temperatures (at different radial locations, Ref. 67), for arc currents 150 and 250 A, respectively. For this investigation, the model is applied to both GMAW of aluminum and iron.

The primary difference to the earlier model application to GMAW of aluminum (Ref. 66) is that the arc column is modeled under the assumption of local thermal equilibrium (LTE). In the earlier model application, non-LTE conditions in the cathode and anode fall regions were accounted for in a simplified way (through source terms in the plasma region close to the anode and the cathode). However, in this investigation the focus is on the majority of the plasma region where LTE exists and not on the small non-LTE boundary layer regions (< 0.1 mm (Ref. 68)). Therefore, we neglect the simplified approach to account for non-LTE boundary regions that was used in the earlier study (Ref. 66).

The paragraphs below summarize the key assumptions, equations, and boundary conditions used in the model. A more detailed description of the mathematical model can be found in an earlier publication (Ref. 66).

Mathematical Formulation

The boundaries of the computational domain for the welding arc are shown in Fig. 4. The system is assumed to be axisymmetric, steady-state and laminar. The plasma is assumed to be at atmospheric pressure, in local thermodynamic equilibrium, optically thin to radiation and the influence of metal droplets is neglected. Also, the consumable electrode is assumed to be cylindrical, and the tip of the electrode and the workpiece surfaces are assumed to be flat.

In applying the above assumptions, the equations, written in cylindrical coordinates, that need to be solved are the conservation of mass, radial and axial momentum, thermal energy, and charge continuity (expressed in the form of the electrical potential). The definitions of the electric potential and Ampere's law are used to calculate the current densities and the self-induced magnetic field, respectively.

The boundary conditions for the welding arc are listed in Table 1 and the variables used in Table 1 are defined in the Appendix. In the anode region (BC, CD in Fig. 4, a no-slip condition is used for the momentum boundary conditions. The enthalpy at the anode h_a is set to the value corresponding to the melting temperature of pure iron (1810 K) or pure aluminum (933 K). The equation for the conservation of charge continuity is the only equation to be solved within the electrode region, and therefore, the electric potential is set to be constant in region DA — Fig. 4. In the region DE, a zero mass-flow gradient dρw/dz was postulated, together with an inlet enthalpy h_i corresponding to a temperature of 300 K. Since it is not clear where inflow (EF) and outflow (FG) will take place in the fringes of the arc column, zero radial mass flow d(ρu)/dr and electric potential gradients were specified. The enthalpy is assumed to correspond to a temperature of 300 K for the gas en-

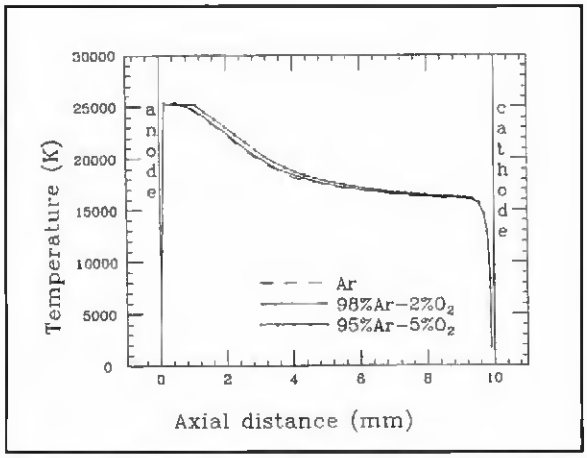

Fig. 15 — The temperature at the center of the arc as a function of the axial distance from the anode.

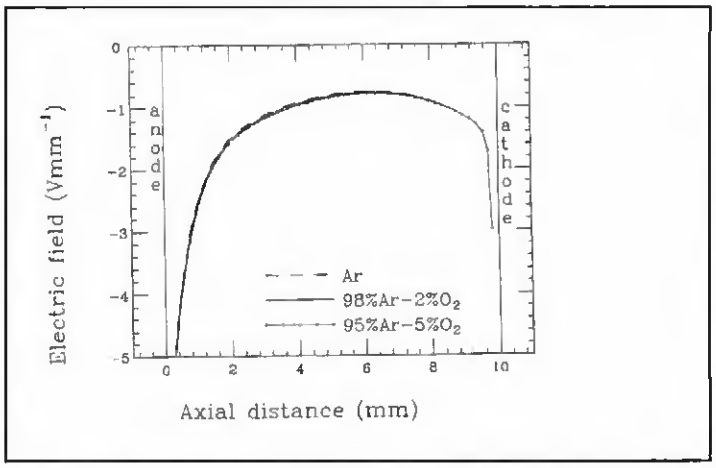

Fig. 16 — The electric field intensity at the center of the arc as a function of the axial distance from the anode.

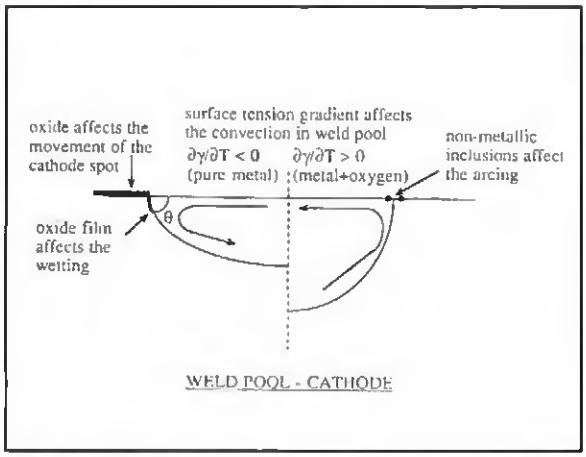

Fig. 17 — The influence of oxygen on phenomena taking place at the workpiece (cathode).

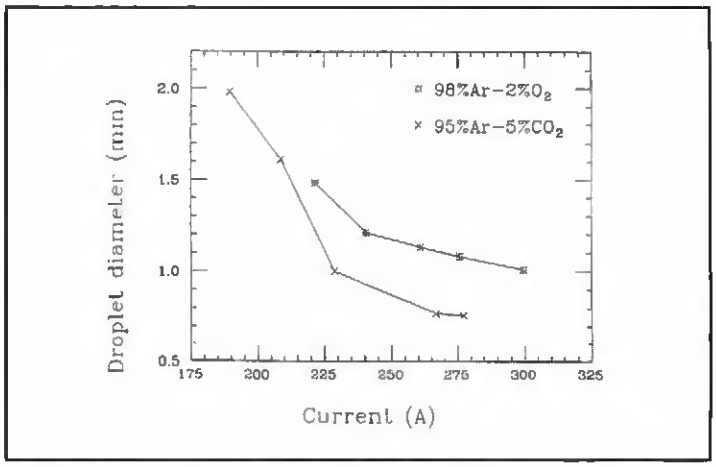

Fig. 18 — The experimentally determined droplet diameter as a function of welding current for a 98% argon - 2% oxygen mixture and a 95% argon - 5% carbon dioxide mixture. The electrode diameter is 1.14 mm.

trained into the system and the enthalpy gradient dh/dr is assumed to be zero for mass flowing out of the system.

In the cathode region (GHI), a no-slip condition is used for the momentum equations. The enthalpies at the cathode surface within $h_{c,i}$ and outside $h_{c,o}$ the weld pool (cathode spot) region are taken at temperature values of 1810 and 1000 K for iron and 933 and 600 K for aluminum, respectively. The radius of the cathode spot R_c, is defined as an average value representing the movement of the cathode spot. Theoretical calculations of the weld pool profiles showed that the weld pool radius in argon-shielded systems is 3.2 to 3.5 mm (0.125 and 0.138 in.) for welding currents of 150 to 220 A (Refs. 27, 28). Based on these values of the weld pool radius, a sensitivity calculation was done to study the effect of the cathode spot radius on the calculated arc characteristics. It was found that the calculated maximum velocity varies less than 1.7% and the maximum temperature varies less than 0.1% for a 2.7 to 4.2 mm (0.11–0.16 in.) range of the cathode spot radius. Therefore, R_c was chosen to be 2.7 mm.

It is assumed that a single value of the current density J_c is valid within the cathode spot (weld pool) region and that the current density is zero outside the cathode spot region. This assumption is based on the strong dependence of the current density on surface temperature; the temperatures in the weld pool region are substantially higher than in the rest of the workpiece. Therefore, the current density conditions at the cathode are given by:

$$J_c = \frac{I}{\pi R_c^2} \qquad r \le R_c \tag{3}$$

$$J_c = 0 \qquad r > R_c \tag{4}$$

Method of Solution

The solution of the governing equations and boundary conditions is obtained by using a modified version of 2/E/FIX, a two-dimensional steady-state code based on a finite volume scheme (Ref. 69). During a calculation, the difference equations are solved by iteration until the residuals are less than 1% of the magnitude of the respective variables. The current balance is satisfied within 1% for all calculations.

Theoretical inputs in the form of thermophysical gas properties are calculated as described earlier. The values of the electrical conductivity of iron and aluminum at their respective melting points are taken from Touloukian (Ref. 70).

Results

Our calculations were done for GMAW of aluminum and iron using the following shielding gases: 1) pure argon; 2) 98% argon - 2% oxygen; and 3) 95% argon - 5% oxygen by weight. The studied range of currents, the arc length and the electrode diameter were 150 to 400 A, 10.0 and 1.2 mm, respectively.

Thermophysical Gas Properties

As mentioned earlier, the thermodynamic and transport properties of the shielding gases were calculated using the program developed at CSIRO (Ref. 47). Figures 5 to 7 show the enthalpy, density and specific heat as a function of temperature. It is obvious from the figures that the addition of oxygen has an insignificant effect on the density, and only small effect on the enthalpy and the specific heat. The largest enthalpy differences occur in the temperature range of 2500 to 12000 K, for which oxygen additions tend to increase the value of the enthalpy slightly. The most noticeable effect of oxygen additions on the specific heat is found at a temperature of 3000 K, where a peak value is found, corresponding to the dissociation of oxygen molecules.

The transport properties; electrical conductivity, thermal conductivity and molecular viscosity; are plotted vs. temperature in Figs. 8–10, respectively. The electrical conductivity is found to increase slightly with increased oxygen

Table 1 — Boundary Conditions for the Arc

Fig. 4	u	w	h	Φ
BC, CD, AD	0	0	h_a	0 (AD)
DE	0	$\frac{\partial \rho w}{\partial z} = 0$	h_i	$\frac{\partial \Phi}{\partial z} = 0$
EG	$\frac{\partial \rho u}{\partial r} = 0$	$\frac{\partial w}{\partial r} = 0$	h_i (inflow) $\frac{\partial h}{\partial r} = 0$ (outflow)	$\frac{\partial \Phi}{\partial r} = 0$
IH	0	0	$h_{c,i}$	Given by Equations 3 and 4
HG	0	0	$h_{c,o}$	0

concentration at temperatures above 22000 K. Similarly, the thermal conductivity and the molecular viscosity are found to increase slightly with oxygen additions for temperatures between 12000 and 20000 K. A small peak occurs in the thermal conductivity of the argon-oxygen mixtures at around 3000 K; this is due to the reaction thermal conductivity associated with the dissociation of oxygen molecules.

Arc Characteristics

The assumptions that are made in the arc model mean that the different anode and cathode materials only influence the arc characteristics through the temperature boundary conditions. More specifically, the different melting temperatures of iron (1810 K) and aluminum (933 K) was the only difference in the models of the iron and aluminum systems. The calculated arc characteristics were found to be independent of this difference in melting temperature. A similar finding has been reported for temperature measurements in the GTAW system; the use of iron or water-cooled copper anodes did not affect the measured temperature profiles (Refs. 71, 72). Our presented results for the characteristics of the arc column are thus valid for both GMAW of iron and aluminum.

The maximum value of the mass flow (ρu) is shown as a function of welding current in Fig. 11. It can be seen that an addition of 5% oxygen to the argon shielding gas decreases the mass flow by between 1.4 and 2.6%. The maximum value of the momentum flux (u^2) is plotted vs. the welding current in Fig. 12. A 95% argon - 5% oxygen gas mixture is found to result in a slightly higher momentum flux, by between 1.3 and 3.4%, in comparison with pure argon. In Fig. 13, the maximum value of the electric potential is shown as a function of the welding current. The addition of 5% oxygen to argon gas increases the value of the electric potential by between 2.8 and 5.1%.

The axial velocity, at the center of the arc and a 250 A welding current, is plotted vs. the axial distance, taken from the anode to the cathode, in Fig. 14. A relatively uniform velocity is found in the arc column, while the velocity decreases dramatically close to the solid anode and cathode surfaces. The addition of 5% oxygen to the argon gas increases the velocity by up to 9.4%. Similarly to Fig. 14, the temperature is plotted vs. the axial distance for a 250 A welding current in Fig. 15. The highest temperatures are found near the anode, where the rate of joule heat generation is highest. The addition of 5% oxygen to the argon gas is found to increase the temperature by a maximum of only 3.8%. Finally, the electric field intensity is shown as a function of axial distance for a 250 A welding current in Fig. 16. The absolute value of the electric field is about 0.8 to 1.0 V mm^{-1} at a location halfway between the anode and the cathode, while it increases in magnitude closer to the anode and the cathode region. The addition of 5% oxygen to the argon gas is found to decrease the magnitude of the electric field intensity by up to 5%.

Comparison of Predicted Arc Characteristics and Experimental Data

As mentioned previously, the predicted arc temperatures were in good agreement with spectroscopically measured temperatures. Besides temperatures, it is also important to compare data of the electrical characteristics, especially since Eagar (Ref. 73) has shown that the majority of the energy transferred to the anode from the welding arc is carried by the current. Such a comparison has recently been done by Jönsson, *et al.* (Ref. 74). However, in this paper, predicted electrical characteristics presented are compared with data from the literature.

The electric potential in the arc column for a pure argon arc is shown to be approximately 13 V at a 200 A welding current — Fig. 13. Adding a voltage drop of 14.9 V for the anode and cathode fall regions (at a 201.9-A welding current, a 8.5-mm (0.33-in.) arc length and a 1.14-mm (0.04 in.) electrode diameter, Ref. 76), gives a total voltage of about 28 V. This is reasonably close to the value of the total voltage of 25 V at a 200-A welding current (data of arc length and electrode diameter are unknown) given by Jackson (Ref. 75). From Fig. 16 it is seen that the absolute value of the predicted electric field intensity is 0.8 to 1.0 V mm^{-1} in the center of the arc. These values agree well with the average values of the electric field intensity of 0.7 to 0.8 V mm-1 reported by Allum (Ref. 76). In that study it was also shown that the electric field intensity increases to 2.5 V mm^{-1} at a distance of 1 mm (0.04 in.) from the cathode. This tendency for the electric field intensity to increase as the cathode is approached is also seen in Fig. 16. However, it should be noted that the accuracy of the predicted values decreases at locations close to the cathode (and the anode), since the influence of the non-LTE cathode fall boundary layer is neglected in the model. As indicated in a recent survey of theoretical welding models (Ref. 77), the theoretical treatment of these non-LTE regions is far from perfected. So far, even the most comprehensive studies modeling the cathode and anode fall regions have used one-dimensional approaches, and they have all been for the related and more studied gas tungsten arc.

Discussion

In the literature review, it was mentioned that it is difficult to strike an arc in a pure argon atmosphere (Ref. 20) and that unstable metal transfer is often observed in these arcs (Ref. 21). The addition of oxygen to the argon shielding gas generally improves the ability to strike an arc and maintain a more stable metal transfer. Up till now, it has not been clear if this is due to effects on the arc characteristics or phenomena at the anode and cathode.

The results shown in Figs. 11–16 indicate that the addition of oxygen to the argon shielding gas has only a small influence on the characteristics of the arc column. The small magnitude of the effect can primarily be explained by the small effect of oxygen additions on the transport and thermodynamic properties of argon, as shown in Figs. 5–10. The absence of major changes to the predicted arc column characteristics indicates that the observed effects of the addition of oxygen to an argon-shielded GMAW process are mainly due to altered transport phenomena at the anode and the cathode. Therefore, it is important to know how oxygen additions to the argon-shielded arc affects the transport phenomena at the cathode and the anode.

Cathode — Workpiece (Weld Pool)

From the literature review, it is clear that the influence of oxygen on the transport phenomena taking place at the cathode has been studied quite extensively. The most important influences of oxygen additions upon phenomena that take place at the workpiece are summarized in Fig. 17. It is seen that the addition of oxygen leads to improved arc stability by: 1) forming nonmetallic inclusions that initiate arcing; and 2) by forming oxides that decrease the movement of the arc (cathode spots). Oxygen also affects the geometry of the weldment by: 1) forming films that improve the wetting conditions of the weld pool; and 2) by affecting the surface tension gradient such that deeper and more narrow weld pools are formed.

Anode — Consumable Electrode

Considerably fewer publications have discussed the influence of oxygen on phenomena taking place at the consumable electrode (anode) than at the cathode. Kim (Ref. 13) studied the melting characteristics of GMAW of iron using pure argon and argon with the addition of 2% oxygen as shielding gases. He found that the presence of oxygen did not affect the melting rate significantly. Similarly, Freeman and Eagar (Ref. 78) studied the same welding system and shielding gases. They found no difference in drop frequency for the pure argon gas and the 98% argon - 2% oxygen mixture. However, they noticed that the average drop size and neck diameter were smaller for the case using pure argon as a shielding gas. Furthermore, the droplets in the pure argon system were more elongated, resembling an elliptical shape. Questioning any assumption that can be made from these results that the addition of oxygen does lead to a larger droplet size, are the results from a further study by Jönsson (Ref. 79). He found that the droplet diameter for a 95% argon–5% carbon dioxide shielding gas mixture is smaller (and the frequency of the droplets is higher) than for a 98% argon–2% oxygen shielding gas mixture at all currents, as is illustrated in Fig. 18.

The 95% argon–5% carbon dioxide shielding gas mixture contains a higher oxygen content than the 98% argon–2% oxygen mixture. Oxygen from the shielding gas can dissolve in the liquid iron as a result of chemical reaction between the gas phase and the liquid iron droplet. The surface tension of liquid iron decreases with an increased oxygen concentration (Ref. 80). Therefore, it is expected that the "oxygen richer" 95% argon–5% carbon dioxide gas mixture lowers the surface tension more than the 98% argon–2% oxygen mixture. The effect of surface tension on droplet detachment can be estimated using the static force balance theory (Refs. 13, 81, 82). This states that a drop detaches from the electrode tip when the static detaching forces (gravitational, electromagnetic and plasma drag forces) exceed the static retaining force due to surface tension. Thus, the observation of smaller droplet sizes and higher droplet frequencies for the argon–carbon dioxide mixture compared to the argon–oxygen mixture in Fig. 18, is explained by the lower value of the surface tension and thereby the lower surface tension retaining force for the argon–carbon dioxide shielding gas.

In summary, the different experimental results reported regarding the influence of oxygen additions on transport phenomena at the anode indicate that a clear understanding of the phenomena involved does not exist. It is an important topic that needs to be investigated further.

Conclusions

The main conclusions of this study can be summarized as follows:

1) The addition of up to 5% oxygen to an argon shielding gas was found to affect the characteristics of the arc column to only a small extent. More specifically, the mass flow, momentum flux, electric potential and temperature were found to change by no more than 5% when oxygen was added to the argon gas.

2) It has been reported that the addition of oxygen to the argon shielding gas affects the general operation of a GMAW process. Since this study has shown that the effect is small in the arc column, it is concluded that the effects are taking place at the anode and cathode regions. The influence of oxygen on the transport phenomena taking place at the cathode has already been studied quite extensively, while more investigation is greatly needed on activity at the anode.

Acknowledgments

Two of the authors, P.G. Jönsson and J. Szekely, wish to thank the Materials Reliability Division at the National Institute of Standards and Technology (NIST) in Boulder, Colo., for financial support of this study.

References

1. Herbst, H. T. and McElrath, T., Jr. 1951. Sigma welding of carbon steels. *Welding Journal* 30(12): 1084–1097.

2. Lancaster, J. F. 1987. The physics of fusion welding, Part 1: The electric arc in welding. IEE Proc.134(5): 233–252.

3. Guile, A. E. 1986. The electric arc. *The Physics of Welding*. ed. J. F. Lancaster, pp. 120–145, Oxford, Pergamon Press.

4. Essers, W .G., and Walter, R. 1980. Some aspects of the penetration mechanisms in metal-inert-gas (MIG) welding. *Arc Physics and Weld Pool Behavior*. ed. W. Lucas, pp. 289–300, The Welding Institute.

5. Smithells, C. J. 1967. *Metals Reference Book* Vol. 1. p. 224, London, Butterworths.

6. Walsh, D. W., and Savage, W. F. 1986. The mechanism of minor element interaction in autogenous weld pools. *Advances in Welding Science and Technology*. ed. S. A. David, pp. 59–63, Gatlinburg, ASM.

7. Kearns, W. H. 1978. *Welding Handbook* Vol. 2. p. 135, Miami, Fla., American Welding Society.

8. Stenbacka, N., and Persson, K.-A. 1989. Shielding gases for gas metal arc welding. *Welding Journal* 68(11): 41–47.

9. Norrish, J. 1992. Advanced Welding Processes. pp. 81–82, Bristol, Institute of Physics Publishing.

10. Francis, R. E., Jones, J. E., and Olson, D. L. 1990. Effect of gas shielding gas oxygen activity on weld metal microstructure of GMA welded microalloyed HSLA steel. *Welding Journal* 69(11): 408-s to 415-s.

11. Guile, A. E. 1984. Electric arcs: their electrode processes and engineering applications. IEE Proc. 131(7): 450–480.

12. Guile, A. E., and Hitchcook, A. H. 1978. *Archiv. für Elektrotechnik*. 60(1): 17–26.

13. Kim, Y.-S. 1989. Metal transfer in gas metal arc welding. Ph.D. Dissertation. Massachusetts Institute of Technology, Cambridge, Mass.

14. Guile, A. E. 1986. The electric arc. *The Physics of Welding*. ed. J. F. Lancaster, pp. 134–135, Oxford, Pergamon Press.

15. Guile, A. E. 1979. Processes at arc cathode roots on nonrefractory metals having films of their own oxide. *Arc Physics and Weld Pool Behavior*. ed. W. Lucas, pp. 79–86, The Welding Institute.

16. Boughton, P., and Amin, M. 1972. Aspects of arc root behavior. 2nd Int. Conf. on Gas Discharges. pp. 130–131, Institution of Electrical Engineers.

17. Lan, F.V. 1979. The dynamics of the arc cathode spot during the welding of an aluminium alloy. Autom. Weld. 32(6): 17–18.

18. Hancox, R. 1960. Importance of insulating inclusions in arc initiation. Brit. J. Appl. Phys. 11(10): 468–471.

19. Pfeil, P. C. L., and Griffiths, L. B. 1959. The effect of inclusions on the arcing behavior of metals. J. Nuclear Mat. 1(3): 244–248.

20. Doan, G. E., and Myer, J. L. 1932. Arc discharge not obtained in pure argon gas. Phys. Rev. 40(4): 36–39.

21. Ries, D. E. 1983. Gas metal arc welding of titanium. S.M. Dissertation, Massachusetts Institute of Technology, Cambridge, Mass.

22. Lucas, W. 1992. Choosing a shielding gas — part 2. *Weld. & Metal Fabrication* 60(7): 269–276.

23. Bradstreet, B. J. 1968. Effect of surface tension and metal flow on weld bead formation. *Welding Journal* 47(6): 314-s to 322-s.

24. Ershov, G. S., and Bychev, V. M. 1975. Influence of gases on the surface tension of liquid iron and low alloy steel. *Russian Metallurgy* (4): 45–46.

25. Popel, S. I., Tsarevskiy, B. V., Pavlov, V. V., and Furman, E. L. 1975. Combined influence of oxygen and sulfur on the surface tension of iron. *Russian Metallurgy* (4): 42-44.

26. Sundell, R. E., Solomon, H. D., and Correa, S. M. 1988. Minor effects on gas tungsten arc (GTA) weld penetration — weld pool physics. *Advances in Welding Science and Technology*. ed. S. A. David, pp. 53–57, ASM.

27. Tsao, K. C., and Wu, C. S. 1988. Fluid flow and heat transfer in GMA weld pools. *Welding Journal* 67(3): 70-s to 75-s.

28. Zacharia, T., Eraslan, A. H., and Aidun, D. K. 1988. Modeling of nonautogenous welding. *Welding Journal* 67(1): 18-s to 27-s.

29. Kim, J.-W., and Na, S.-J. 1991. A study of the three-dimensional analysis of heat and fluid flow in gas metal arc welding using boundary-fitted coordinates. *Weld. and Joining Proc.* eds. E. Kannatey-Asibu Jr, H. S. Cho and S. Fukuda, pp. 159–173, ASME.

30. Oreper, G. M., Eagar, T. W., and

Szekely, J. 1983. Convection in arc weld pools. *Welding Journal* 62(11): 307-s to 312-s.

31. Oreper, G. M., and Szekely, J. 1984. Heat-and fluid-flow phenomena in weld pools. *J. Fluid. Mech.* 147: 53–79.

32. Kou, S., and Sun, D. K. 1985. Fluid flow and weld penetration in stationary arc welds. *Met. Trans. A.* 16A(2): 203–213.

33. Oreper, G. M., Szekely, J., and Eagar, T. W. 1986. The role of transient convection in the melting and solidification in arc weld pools. *Met. Trans. B.* 17B(12): 735–744.

34. Correa, S. M., and Sundell, R. E. 1986. A computational and experimental study of the fluid flow in weld pools. *Modeling and Control of Casting Processes.* eds. S. Kou and R. Mehrabian, pp. 211–227, TMS-AIME.

35. Matsunawa, A., Yokoya, S., and Asako, Y. 1987. Convection in weld pool and its effect on penetration shape in stationary arc welds. Trans. *J.W.R.I.* 16(2): 229–236.

36. Oreper, G. M., and Szekely, J. 1987. A comprehensive representation of transient weld pool development in spot welding operations. *Met. Trans. A.* 18A(7): 1325–1332.

37. Heiple, C. R., and Roper, J. R. 1982. Mechanism for minor element effect on GTA fusion zone geometry. *Welding Journal.* 61(4): 97s-102s.

38. Sahoo, P., Debroy, T., and McNallan, M. J. 1988. Surface tension of binary metal — surface active solute systems under conditions relevant to welding metallurgy. *Met. Trans. B* 19B(6): 483–491.

39. Zacharia, T., David, S. A., Vitek, J. M., and Debroy, T. 1989. Weld pool development during GTA and laser beam welding of type 304 stainless steel, Part I — theoretical analysis. *Welding Journal* 68(12): 499-s to 509-s.

40. Zacharia, T., David, S. A., Vitek, J. M., and Debroy, T. 1989. Weld pool development during GTA and laser beam welding of type 304 stainless steel, Part II - Experimental correlation. *Welding Journal* 68(12): 510-s to 519-s.

41. Zacharia, T., David, S. A., and Vitek, J. M. 1991. Effect of evaporation and temperature-dependent material properties on weld pool development. *Met. Trans. B* 22B(4): 233–241.

42. Zacharia, T., David, S. A., Vitek, J. M., and Kraus, H. G. 1991. Computational modeling of stationary gas-tungsten-arc weld pools and comparison to stainless steel 304 experimental results. *Met. Trans. B* 22B(4): 243–257.

43. Evans, D. L., and Tankin, R. S. 1967. Measurement of emission and absorption of radiation by an argon plasma. *Phys. Fluids* 10(6): 1137–1144.

44. Krey, R. U., and Morris, J. C. 1970. Experimental total line radiation of nitrogen, oxygen, and argon plasmas. *Phys. Fluids* 13(6): 1483–1487.

45. Gordon, S., and McBride, B. J. 1971. Computer program for calculation of complex chemical equilibrium compositions, rocket performance, incident and reflected shocks, and Chapman-Jouguet detonations. Special Publication SP-273, Washington DC, NASA.

46. Svehla, R. A., and McBride, B. J. 1973. Fortran IV computer program for calculation of thermodynamic and transport properties of complex chemical systems. Technical Note TN D-7056, Washington DC, NASA.

47. Kovitya, P. 1982. Theoretical determination of material functions of plasmas formed from ablated PTFE, alumina, PVC, and perspex for the temperature range of 5000 to 30000 K. Technical Memorandum No. 3, Sydney, Australia, CSIRO Division of Applied Physics.

48. Kovitya, P. 1984. Thermodynamic and transport properties of ablated vapors of PTFE, alumina, perspex and PVC in the temperature range 5000 to 30000 K. *IEEE Trans. Plasma Sci.* 12:38–42.

49. Kovitya, P. 1985. Physical properties of high-pressure plasmas of hydrogen and copper in the temperature range 5000 to 60000 K. *IEEE Trans. Plasma Sci.* 13: 587–594.

50. Moore, C. E. 1949. Atomic energy levels. Circular 467, Vol I, pp. 45–53 and 211–220, Washington DC, US National Bureau of Standards.

51. Chase, M. W., Jr, Davies, C. A., Downey, J. R. Jr, Frurip, D. J., McDonald, R. A., and Syverud, A. N. 1985. JANAF thermochemical tables. *J. Phys. Chem.* Ref. Data 14, Suppl. 1.

52. Hirschfelder, J.O., Curtiss, C.F., and Bird, R.B. 1964. *Molecular Theory of Gases and Liquids.* 2nd ed., New York, Wiley.

53. Chapman, S., and Cowling, T. G. 1970. *The Mathematical Theory of Non-Uniform Gases.* 3rd ed., Cambridge, UK, Cambridge University Press.

54. Ferziger, J. H., and Kaper, H. G. 1972. The Mathematical Theory of Transport Processes in Gases. Amsterdam, North-Holland.

55. Murphy, A. B. 1994. Transport coefficients of argon, nitrogen, oxygen, argon-nitrogen and argon-oxygen plasmas. *Plasma Chem. Plasma Process.*

56. Devoto, R. S. 1967. Transport coefficients of partially ionized argon. *Phys. Fluids.* 10: 354–364.

57. Devoto, R. S. 1967. Simplified expressions for the transport properties of ionized monoatomic gases. *Phys. Fluids* 10:2105–2112.

58. Aubreton, J., Bonnefoi, C., and Mexmain, J. M. 1986. Calcul de proprietes thermodynamiques et des coefficients de transport dans un plasma Ar-O_2 en non-equilibre thermodynamique et a la pression atmosperique. *Rev. Phys. Appl.* 21: 365–376.

59. Aziz, R. A., and Slaman, M. J. 1990. The repulsive wall of the Ar-Ar interatomic potential reexamined. *J. Chem. Phys.* 92: 1030–1035.

60. Pirani, F., and Vecchiocattivi, F. 1981. The interaction potential energy surface of O_2 - Ar. *J. Chem. Phys.* 59: 387–396.

61. Rutherford, J. A., and Vroom, D. A. 1974. The reaction of atomic oxygen with several atmospheric ions. *J. Chem. Phys.* 61: 2514–2519.

62. Levin, E., Partridge, H., and Stallcop, J. R. 1990. Collision integrals and high-temperature transport properties for N-N, O-O, and N-O. J. Thermophys. *Heat Transf.* 4: 469–477.

63. Stallcop, J. R., Partridge, H., and Levin, E. 1991. Resonance charge transfer, transport cross-sections, and collision integrals for N+(3P)-N(4S0) and O+(4SO)-O(3P) interactions. J. Chem. Phys. 95:6429–6439.

64. Itikawa, Y. 1974. Momentum-transfer cross-sections for electron collisions with atoms and molecules. *At. Data Nucl. Data Tables* 14: 1–10.

65. Itikawa, Y. 1978. Momentum-transfer cross-sections for electron collisions with atoms and molecules. Revisions and supplement, 1977. *At. Data Nucl. Data Tables* 21: 69–75.

66. Jönsson, P. G., Westhoff, R. C., and Szekely, J. 1993. Arc characteristics in gas metal arc welding of aluminum using argon as shielding gas. J. Appl. Phys. 74(10):5997–6006.

67. Smårs, E. A., and Acinger, K. 1968. Material transport and temperature distribution in arc between melting aluminum electrodes. Report No. 212-162-68, International Institute of Welding.

68. Finkelnburg, W., and Segal, S. M. 1951. The potential field in and around a gas discharge, and its influence on the discharge mechanism. *Phys. Rew.* 83(3):582–585.

69. Pun, W. M., and Spalding, D. B. 1976. A general computer program for two-dimensional elliptic flows. Rep. No. HTS/76/2, Heat Transfer Section, Dept. of Mechanical Engineering, Imperial College, London.

70. Touloukian, Y. S. 1967. *The Elements, Thermophysical Properties of High Temperature Solid Materials.* pp. 9 and 581, New York, Macmillan Co.

71. Farmer, A. J. D., Haddad, G. N., and Cram, L. E. 1986. Temperature determinations in a free-burning arc. III: Measurements with molten anodes. *J. Phys. D.* 19:1723-1730.

72. Gick, A. E. F., Quigley, M. B. C., and Richards, P. H. 1973. The use of electrostatic probes to measure the temperature profiles of welding arcs. *J. Phys. D.* 6: 1941–1949.

73. Eagar, T.W. 1990. An iconoclast's view of the physics of welding - rethinking old ideas. Recent Trends in Welding Research. eds. S. A. David and J. M. Vitek, pp. 1-6, ASM.

74. Jönsson, P. G., Szekely, J., Madigan, R. B., and Quinn, T. P. 1994. Power characteristics in GMAW: Experimental and numerical investigation. *Welding Journal,* In press.

75. Jackson, C. E. 1960. The science of arc welding. Part II — consumable-electrode welding arc. *Welding Journal* 40(5):177-s to 190-s.

76. Allum, C. J. 1983. Power dissipation in the column of a TIG welding arc. *J. Phys. D: Appl. Phys.* 16:2149–2165.

77. Jönsson, P. G., Szekely, J., Choo, R. T. C., and Quinn, T. P. 1994. Mathematical models of transport phenomena associated with arc welding processes: A survey. *Modelling Simul. Mater. Sci. Eng.* 2:995–1016.

78. Freeman, J. J., and Eagar, T. W. 1992. An investigation of gas metal arc welding of steel in pure argon, Interim Report, Materials Processing Center, Massachusetts Institute of Technology, Cambridge, Mass.

79. Jönsson, P. G. 1993. Arc properties and metal transfer in gas metal arc welding D.Sc. Dissertation, Massachusetts Institute of Technology, Cambridge, Mass.

80. Heiple, C. R., and Roper, J. R. 1982. Mechanism for minor element effect on GTA fusion zone geometry. *Welding Journal* 61(4):97-s to 102-s.

81. Greene, W. J. 1960. An analysis of transfer in gas-shielded welding arcs. Trans. AIEE part 2 7:194–203.

82. Waszink, J. H., and Graat, L. H. J. 1983. Experimental investigation of the forces

acting on a drop of weld metal. *Welding Journal* 62:108-s to 116-s.

Appendix

Nomenclature

a_o Activity of oxygen (-)
A Constant in the surface tension coefficient ($Nm^{-1}K^{-1}$)
h Plasma enthalpy (Jkg^{-1})
h_a Enthalpy at the anode (Jkg^{-1})
h_i Enthalpy of gas flowing into the system (Jkg^{-1})
$h_{c,i}$ Enthalpy at the cathode surface within the cathode spot region (Jkg^{-1})
$h_{c,o}$ Enthalpy at the cathode surface outside the cathode spot region (Jkg^{-1})
I Welding current (A)
J_c Cathode current density (Am^{-2})
K_{seg} Equilibrium constant for segregation (-)
M_j Molecular weight of the jth species ($kgmol^{-1}$)
P Pressure (Nm^{-2})
r Radial distance (m)
R Gas constant ($Jmol^{-1}K^{-1}$)
R_c Cathode spot (weld pool) radius (m)
T Temperature (K)
u Radial velocity (ms^{-1})
w Axial velocity (ms^{-1})
x_j Mole fraction of the jth species (-)
z Axial distance (m)

Greek Symbols

ΔH^0 Standard heat of adsorption ($Jmol^{-1}$)
ρ Density (kgm^{-3})
Φ Electric potential (V)
γ Surface tension (Nm^{-1})
γ_l Surface tension of liquid metal (Nm^{-1})
γ_s Surface tension of solid metal (Nm^{-1})
γ_{sl} Solid/liquid interfacial tension (Nm^{-1})
Γ_0 Surface excess at saturation ($molm^{-2}$)
θ Wetting contact angle (degrees)